netic oxygen molecules that were strongly attracted to the surfaces of SWNT bundles. However, partial contribution due to possible changes of electronic properties (i.e., they became more metallic) cannot be excluded. This issue is currently under systematic investigation. Nevertheless, interactions between SWNTs and oxygen molecules at room temperature cannot be ignored.

References and Notes

1. J. W. Mintmire, B. I. Dunlap, C. T. White, *Phys. Rev. Lett.* **68**, 631 (1992).
2. R. Saito, M. Fujita, G. Dresselhaus, M. S. Dresselhaus, *Appl. Phys. Lett.* **60**, 2204 (1992).
3. J. W. G. Wildoer, L. C. Venema, A. G. Rinzler, R. E. Smalley, C. Dekker, *Nature* **391**, 59 (1998).
4. T. W. Odom, J.-L. Huang, P. Kim, C. M. Lieber, *Nature* **391**, 62 (1998).
5. A. Thess *et al.*, *Science* **273**, 483 (1996).
6. O. Zhou, B. Gao, C. Bower, L. Fleming, H. Shimoda, *Mol. Cryst. Liq. Cryst.*, in press.
7. Supplemental data, figures, and discussions are available at *Science* Online at www.sciencemag.org/feature/data/1048140.shl
8. T. Yildirim, O. Zhou, J. E. Fischer, *Fullerene-Based Materials*, W. Andreoni, Ed. (Kluwer Academic, Dordrecht, Netherlands, in press).
9. H. Kataura *et al.*, *Jpn. J. Appl. Phys.* **37**, L616 (1998).
10. NMR measurements were done in a field of 9.4 T. The ^{13}C T_1 was measured by the saturation-recovery method with pulsed spin-locking detection. Intensity calibration showed that the observable ^{13}C nuclei are over 80% in sample C. Paramagnetic centers, which might wipe out spins in the surrounding and experimental errors, such as the sample dependence of the Q factor, may contribute to the small discrepancy.
11. The MAS spectra taken at various recovery times after a saturation pulse in sample C reveal a broad featureless peak, which has a short spin-lattice relaxation time of 0.5 s at room temperature. This peak is about 30% of the total intensity and is attributed to impurities in sample C.
12. J. Winter, *Magnetic Resonance in Metals* (Clarendon, Oxford, 1971).
13. Although $T_{1\beta}$ is comparable to the lowest ^{13}C T_1 value observed in graphite (100 to 1000 s at 300 K), the concentration of graphite and carbon nanoparticles in the present sample is too small to account for the observed two-thirds of the ^{13}C nuclear spins. Furthermore, the residual Ni particles are generally wrapped in carbon nanoparticles, which would be wiped out from the NMR signal by local magnetic field. Therefore, ^{13}C nuclei associated with both $T_{1\alpha}$ and $T_{1\beta}$ were attributed to SWNTs.
14. R. Tycko *et al.*, *Phys. Rev. Lett.* **68**, 1912 (1992).
15. V. P. Antropov, I. I. Mazin, O. K. Andersen, A. I. Liechtenstein, O. Jepsen, *Phys. Rev. B* **47**, R12373 (1993).
16. C. H. Pennington *et al.*, *Phys. Rev. B* **53**, R2967 (1996).
17. C. H. Pennington and V. A. Stenger, *Rev. Mod. Phys.* **68**, 855 (1996).
18. The ratio $T_{1\beta}/T_{1\alpha} = 8$ far exceeds the largest ratio of 2.5 between the fastest and the slowest relaxation rate due to the anisotropy of the relaxation mechanism (*16*). Thus, the nonexponential decay is due to the distribution of tube properties, rather than the relaxation mechanism. However, each of the two components can be nonexponential due to the anisotropic relaxation mechanism as well as the distribution of tube diameters. Such details, however, cannot be revealed by data. If the decay is not strictly exponential, $1/T_{1\alpha}$ should be a good estimate of the decay rate at early time, and this is equal to $\langle 1/T_1 \rangle_{avg}$ [see (*16*)].
19. J. W. Mintmire and C. T. White, *Appl. Phys. A* **67**, 65 (1998).
20. C. L. Kane and E. J. Mele, *Phys. Rev. Lett.* **78**, 1932 (1997).
21. J. W. Mintmire and C. T. White, *Phys. Rev. Lett.* **81**, 2506 (1998).
22. Often, the distribution of relaxation rate was described by a stretched exponential function $M^* = \exp[-(t/\tau)^{\beta}]$, although here the double-exponential fit is generally better (*7*). However, both these points of views describe distribution of tube properties and differ only quantitatively in nature.

23. We thank H. Kataura for helpful discussion and J. Lorentzen and L.E. McNeil for assistance in Raman measurement. Supported by the U.S. Office of Naval Research and the NSF.

21 December 1999; accepted 3 March 2000

Crossed Nanotube Junctions

M. S. Fuhrer,[1] J. Nygård,[1] L. Shih,[1] M. Forero,[1] Young-Gui Yoon,[1] M. S. C. Mazzoni,[1] Hyoung Joon Choi,[2] Jisoon Ihm,[2] Steven G. Louie,[1] A. Zettl,[1] Paul L. McEuen[1]*

Junctions consisting of two crossed single-walled carbon nanotubes were fabricated with electrical contacts at each end of each nanotube. The individual nanotubes were identified as metallic (M) or semiconducting (S), based on their two-terminal conductances; MM, MS, and SS four-terminal devices were studied. The MM and SS junctions had high conductances, on the order of 0.1 e^2/h (where e is the electron charge and h is Planck's constant). For an MS junction, the semiconducting nanotube was depleted at the junction by the metallic nanotube, forming a rectifying Schottky barrier. We used two- and three-terminal experiments to fully characterize this junction.

Single-walled carbon nanotubes (SWNTs) have been proposed as an ideal system for the realization of molecular electronics (*1*). Individual SWNTs may act as devices such as field-effect transistors (*2, 3*), single-electron-tunneling transistors (*4, 5*), or rectifiers (*6–10*). However, a question remains: How can individual SWNTs be joined together to form multiterminal devices and, ultimately, complex circuits? We have begun to address this question by characterizing SWNT-SWNT junctions formed by nanotubes that lie across one another on a substrate. This type of junction is easily constructed and, with the development of techniques to place nanotubes with precision on substrates (*11*), could conceivably be mass produced.

Our SWNT-SWNT junctions consist of two crossed individual SWNTs or small bundles (diameter <3 nm) of SWNTs with four electrical contacts, one on each end of each SWNT or bundle (*12*). In addition, a gate voltage V_g can be applied to the substrate to change the charge density per unit length of the SWNTs. In an atomic force microscope (AFM) image of a completed crossed nanotube device (Fig. 1), two crossed SWNTs (green) interconnect the Cr/Au contacts (yellow).

We can independently measure each SWNT and determine its properties in this configuration. SWNTs may be metallic or semiconducting, depending on their chirality (*13*). At room temperature, metallic SWNTs have a finite conductance that is nearly independent of V_g. Semiconducting SWNTs are found to be *p*-type, conducting at negative V_g and insulating at positive V_g (*2*). Our crossed SWNT can be composed of two metallic SWNTs (MM), one metallic and one semiconducting SWNT (MS), or two semiconducting SWNTs (SS).

The two-terminal conductances measured across MM junctions are comparable to the two-terminal conductances of the individual SWNTs; the junction resistance is of the same order of magnitude as that of the tubes and their metallic contacts. This result prompted us to measure the four-terminal conductances of the crossed SWNT devices in order to accurately determine the junction conductance. Current is passed into one arm of one tube and sunk from one arm of the second tube. The other arms act as voltage probes. Figure 2A shows the four-terminal current-voltage (I-V) characteristic of an MM junction at 200 K (*14*). The slope of IV corresponds to a resistance of 200 kilohm, or a conductance G of 0.13 e^2/h (where e is the electron charge and h is Planck's constant). Similar measurements of three other MM junctions gave conductances of 0.086, 0.12, and 0.26 e^2/h.

The measured conductances of MM junctions correspond to a transmission probability for the junction $T_j = G/(4e^2/h) \approx 0.02$ to 0.06. Thus, an electron arriving at the junction in one SWNT has chance of a few percent of tunneling into the other SWNT. MM junctions make surprisingly good tunnel contacts, despite the extremely small junction area (on the order of 1 nm^2). We have performed first-principles density functional calculations of the conductance of MM junctions (*15*) (see supplementary material

[1]Department of Physics, University of California at Berkeley and Materials Sciences Division, Lawrence Berkeley National Laboratory, Berkeley, CA 94720, USA. [2]Department of Physics and Center for Theoretical Physics, Seoul National University, Seoul 151-742, Korea.

*To whom correspondence should be addressed. E-mail: mceuen@socrates.berkeley.edu

available at *Science* Online at www.sciencemag.org/feature/data/1048209.shl). For two SWNTs with wrapping indices (5,5) separated by the van der Waals distance of 0.34 nm (Fig. 1B), we find $T_j \approx 2 \times 10^{-4}$. However, when the contact force between the nanotubes due to interaction with the SiO_2 substrate was included (*16*) (Fig. 1C), we found that the nanotubes deformed significantly at the junction. In this case, we found $T_j \approx 0.04$, in excellent agreement with the experimental result. Indeed, the charge density in the contact region became sizeable as the nanotubes became closer and more deformed, resulting from a significant overlap of intertube wavefunction.

The measurements of SS junctions are complicated by the often very resistive (*3*) contacts to semiconducting SWNTs. Nevertheless, we have observed two terminal conductances of SS junctions as high as 0.011 e^2/h and 0.06 e^2/h (the higher conductance curve is represented by the open circles in Fig. 2A). These values are lower bounds for the true SS junction conductances and indicate that the SS junctions, like the MM junctions, make relatively good tunnel contacts. This result is not surprising; both MM junctions (Fig. 2B) and SS junctions (Fig. 2C) are expected to have a finite density of states available for tunneling on either side of the junction.

The MS case (Fig. 2D) is qualitatively different from the MM and SS cases. Charge transfer at the junction between a doped semiconducting SWNT and a metallic SWNT is expected to form a Schottky barrier (*17*) as follows. Because semiconducting and metallic SWNTs both share the same graphene band structure, we expect them to have nearly identical work functions. Hence, the Fermi level E_F of the metallic SWNT should align within the band gap of the semiconducting SWNT at the junction, depleting the doping of the semiconducting SWNT at the junction. Far from the junction, however, E_F is in the valence band of the semiconducting SWNT.

Thus, in addition to the tunnel barrier between the two SWNTs, there also exists a Schottky barrier with a height approximately equal to half the band gap of the semiconducting SWNT. The depletion region in the semiconducting SWNT associated with the Schottky barrier represents an additional tunneling barrier. The total barrier transmission probability T_{MS} is then given by $T_{MS} \approx T_j T_d$, where T_d is the transmission probability for tunneling through the depletion region to the location of the metal SWNT, and T_j is the probability of tunneling between the SWNTs.

The *I-V* curves for two MS junctions, measured at a temperature of 50 K and $V_g = -25$ V, are also shown in Fig. 2A. We first concentrate on the linear response conductance of the MS junctions. Compared with the MM and SS junctions, the low-bias conductances are two orders of magnitude smaller; $T_{MS} \approx 2 \times 10^{-4}$ for both devices. If we assume that $T_j \approx 0.04$ for the MS junctions (which is comparable to the MM value), then $T_d \approx 5 \times 10^{-3}$ (*18*). This is in excellent agreement with a recent calculation by Odintsov (*17*), who found $T_d \approx 5 \times 10^{-3}$ and a corresponding depletion width of 7 nm for a doping level similar to that of our experimental case (*19*).

The *I-V* characteristics of the two MS devices shown in Fig. 2A are shown over an expanded bias range in Fig. 3A. The conductance grows with increasing bias and is greater for positive biases applied to the semiconducting SWNT than for negative biases. (The two

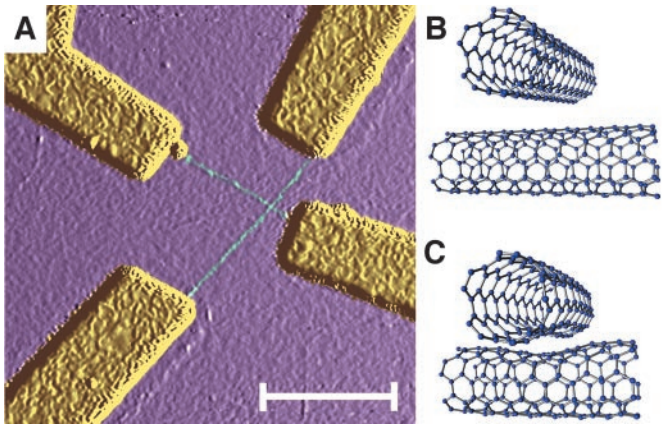

Fig. 1. (**A**) Tapping-mode AFM image (amplitude signal) of a crossed SWNT device. Two SWNTs (green) can be seen spanning between the Cr/Au electrodes (yellow). (**B** and **C**) The structures used to calculate the conductance of a junction between two metallic (5,5) SWNTs (see text and supplementary material).

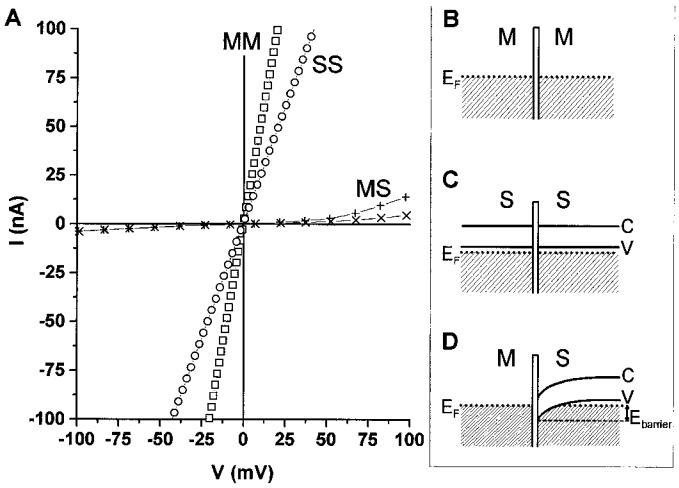

Fig. 2. (**A**) *I-V* characteristics of several SWNT junctions. Open squares, four-terminal measurement of an MM at 200 K; open circles, two-terminal measurement of an SS at 200 K; crosses and plus signs, two-terminal measurements of MS junctions at 50 K and $V_g = -25$V. (B through D) The expected band structures near the junctions. There exists a finite density of states on either side of the junction for (**B**) the MM and (**C**) the SS junctions. (**D**) In the MS junction, a Schottky barrier of height $E_{barrier}$ forms in the semiconducting SWNT because of charge transfer from the metallic SWNT. (The conduction and valence bands of the semiconducting SWNTs are denoted by *C* and *V* and the Fermi level by E_F).

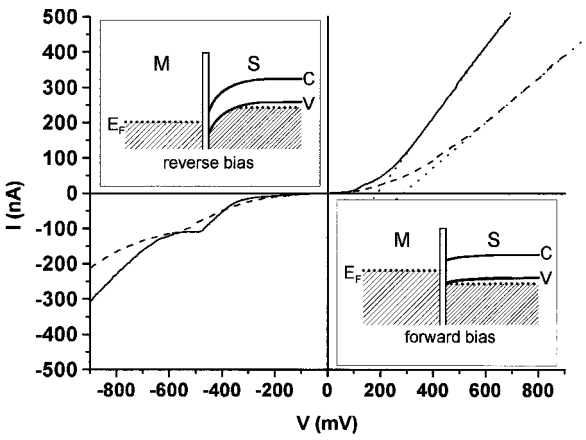

Fig. 3. Two-terminal *I-V* characteristics of two metallic SWNT–semiconducting SWNT junctions at a temperature of 50 K (solid and dashed lines). Bias was applied to the semiconducting SWNT. The dotted lines are linear fits to the forward bias data. The schematic energy level diagrams for the reverse bias (upper left inset) and forward bias (lower right inset) are shown.

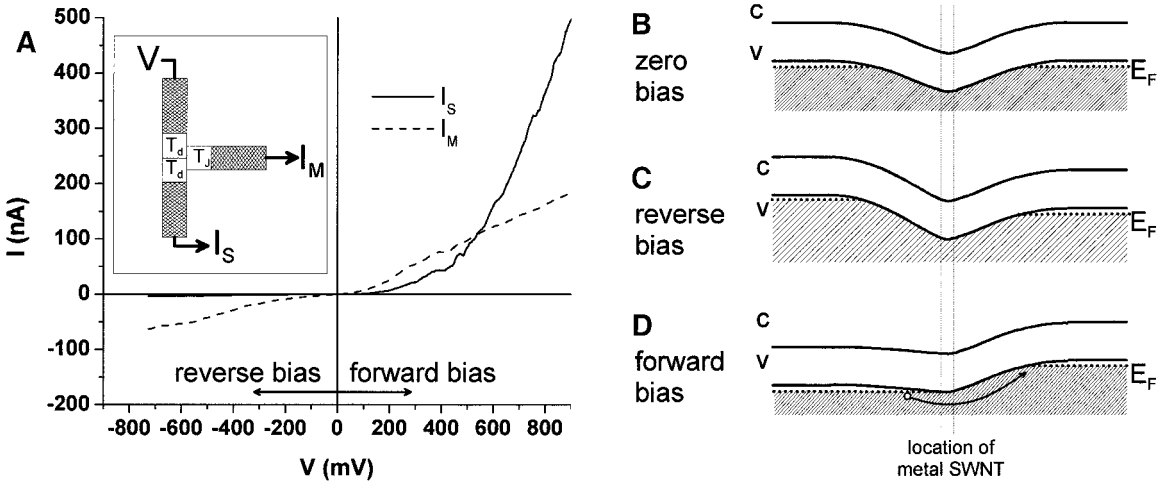

Fig. 4. (**A**) Three-terminal measurement of a metallic SWNT–semiconducting SWNT device at 100 K. I_M, current flowing from metallic SWNT; I_S, current flowing from semiconducting SWNT. The inset (upper left) shows the measurement configuration (for simplicity, only one terminal of the metallic SWNT is shown). (**B**) At zero bias, a conduction barrier exists in the semiconducting SWNT, caused by depletion of carriers by the metallic SWNT at the junction. (**C**) In reverse bias, the barrier between the grounded metallic SWNT and the grounded end of the semiconducting SWNT persists. (**D**) In forward bias, the barrier disappears when the potential difference between the left end of the semiconducting SWNT and the metallic SWNTis equal to the barrier height. Current is then free to flow in the semiconducting SWNT, as seen in (A).

terminal *I-V* curves of MM and SS junctions are relatively featureless over the same bias range.) This nonlinear behavior is expected for a Schottky barrier formed at the junction between a metal and a *p*-type semiconductor: Forward biases reduce the Schottky barrier (Fig. 3, lower inset) and lead to current flow. The forward-bias *I-V* curve saturates to a linear behavior, which extrapolates to a positive *V* intercept. The *V* intercept of the linear region gives a measure of the barrier height: $E_{\text{barrier}} = 190$ and 290 meV for the two devices. This agrees reasonably well with the expected barrier height $E_{\text{barrier}} = E_g/2 \sim 250$ to 350 meV for 1- to 1.5-nm semiconducting SWNTs ($E_g \sim 500$ to 700 meV) (*13*). Reverse biases increase the Schottky barrier (Fig. 3, upper inset), but because the depletion region is small, tunneling still occurs through the barrier and leads to a measurable current flow that increases with increasing reverse bias.

The depletion region in the semiconducting SWNT at the junction should have an even more profound effect on the conductance through the semiconducting SWNT itself, because in this case charge carriers must pass a barrier twice as wide as in tunneling to the metallic SWNT (Fig. 4B). The semiconducting SWNT contains two barriers, each with transmission probability T_d, corresponding to the depletion regions in the semiconducting SWNT on either side of the metallic SWNT. The total transmission through the semiconducting SWNT is then given by $T_S \approx T_d^2$.

We explore this effect using the following device geometry. A voltage was applied to one end of the semiconducting SWNT in an MS device, while the other end was grounded through a current-measuring amplifier. A second amplifier measured the current flowing to ground through the metallic SWNT (inset, Fig. 4A). The three-terminal geometry allows for the determination of the direct transmission through the semiconducting SWNT, T_S, excluding processes that involve the transmission through the metal SWNT. The linear response conductance across the semiconducting SWNT is 4.3 nS, corresponding to a transmission probability $T_S = 2.8 \times 10^{-5}$. This indicates that $T_d \approx (T_S)^{1/2} \approx 5.3 \times 10^{-3}$, in excellent agreement with the two-terminal result $T_d \approx 5 \times 10^{-3}$ obtained earlier. These results quantitatively verify our description of the nature of the MS junction in crossed SWNTs.

The potential of the metal SWNT electrode may be used to control the nonlinear characteristics of the semiconducting SWNT. We can ground the metal SWNT as well as one end of the semiconducting SWNT (Fig. 4A). When a negative voltage is applied, the barrier to holes will remain intact, because the metallic SWNT remains at roughly the same potential as the grounded end of the semiconducting SWNT (Fig. 4C). However, when a positive bias is applied so that the potential difference between the metallic and semiconducting SWNT is greater than the barrier height, holes may pass the barrier and current will flow through the semiconducting SWNT (Fig. 4D). We observed such a response in the measured current leaving the semiconducting SWNT (I_S in Fig. 4A).

The current from the semiconducting SWNT is approximately 100 times greater for a bias of +700 mV than for −700 mV. The direction of the rectification is determined by the contact of the semiconducting SWNT to which the metal SWNT is connected. It has been noted that the ineffective screening inherent in one-dimensional systems poses problems for nanotube Schottky devices (*20*): Nanometer-scale depletion regions are likely to be leaky barriers to tunneling. The existence of a third terminal in our MS junction device offers a solution to this problem, allowing us to construct a good rectifier from narrow Schottky barriers. The active length of our device is on the order of 15 nm, demonstrating that useful devices consisting of only a few thousands of atoms can be constructed from SWNTs.

References and Notes

1. C. Dekker, *Phys. Today* **52**, 22 (1999).
2. S. J. Tans, R. M. Verschueren, C. Dekker, *Nature* **393**, 49 (1998).
3. R. Martel *et al.*, *Appl. Phys. Lett.* **73**, 2447 (1998).
4. S. J. Tans *et al.*, *Nature* **386**, 474 (1997).
5. M. Bockrath *et al.*, *Science* **275**, 1922 (1997).
6. P. Lambin *et al.*, *Chem. Phys. Lett.* **245**, 85 (1995).
7. R. Saito, G. Dresselhaus, M. S. Dresselhaus, *Phys. Rev. B* **53**, 2044 (1996).
8. L. Chico *et al.*, *Phys. Rev. Lett.* **76**, 971 (1996).
9. P. Collins *et al.*, *Science* **278**, 100 (1997).
10. Z. Yao *et al.*, *Nature* **402**, 273 (1999).
11. J. Liu *et al.*, *Chem. Phys. Lett.* **303**, 125 (1999).
12. Samples were fabricated on a backgated substrate consisting of degenerately doped silicon capped with 1 μm of SiO_2. Cr/Au alignment marks were defined on the SiO_2 surface by electron beam lithography. SWNTs synthesized by laser ablation were ultrasonically suspended in dichloroethane, and the resulting suspension was placed on the substrate for approximately 15 s, then washed off with isopropanol. An AFM operating in tapping mode was used to locate favorably arranged, crossed SWNTs relative to the alignment marks on the substrate. Objects whose height profile was consistent with single SWNTs (≈1.4 nm) were preferentially selected, but some devices consisting of small bundles of SWNTs (<3 nm) were also fabricated, with similar results. After locating the desired SWNT crosses, electron beam resist [poly(methylmethacrylate)] was applied over the substrate, and Cr/Au electrical contacts were fabricated on top of the SWNTs using a standard liftoff electron beam lithography technique.
13. M. S. Dresselhaus, G. Dresselhaus, P. C. Eklund, *Science of Fullerenes and Carbon Nanotubes* (Academic Press, San Diego, CA, 1996).
14. We expect that the temperature dependence of the MM junction tunnel conductance should show signatures of Luttinger Liquid (LL) effects [M. Bockrath *et al.*, *Nature* **397**, 598 (1999); Z. Yao, H. W. Ch. Postma, L. Balents, C. Dekker, *Nature* **402**, 273 (1999)]. How-

ever, we observe a somewhat stronger temperature dependence than that expected for LL-LL tunneling in MM junctions measured at low temperatures, most likely due to Coulomb blockade in the individual SWNTs.
15. R. Landauer, *IBM J. Res. Dev.* **1**, 223 (1958).
16. T. Hertel, R. E. Walkup, P. Avouris, *Phys. Review B* **58**, 13870 (1998).
17. A. A. Odintsov, preprint (1999).
18. At our experimental temperatures, we expect tunneling to be the dominant mechanism for conduction across the barrier in linear response: The Boltzmann factor for thermal activation of carriers is less than 10^{-4} at $T < 300$ K and $E_{barrier} = 250$ meV. We observe only weak temperature dependence of the conductance in our MS devices above 50 K.
19. In our devices, the gate voltage changes the charge state of the SWNT by approximately 2×10^5 electrons per volt per centimeter of SWNT. This corresponds to a doping level of $\sim 5 \times 10^6$ holes/cm at a gate voltage of -25 V, or a Fermi level of ~ 75 meV referenced to the valence band. For a SWNT 1.4 nm in diameter, this corresponds to a doping level of $\Delta \approx 1.3$ in the terminology of (*17*) and $f \approx 3 \times 10^{-3}$ in the terminology of (*20*).
20. J. Leonard and F. Tersoff, *Phys. Rev. Lett.* **83**, 5174 (1999).
21. We thank U. Varadarajan, A. K. L. Lim, and M. Bockrath for useful discussions and help with the experimental details of this work, and A. Rinzler and R. E. Smalley for providing the SWNT material used in this study. Supported by the sp² Materials Initiative (U.S. Department of Energy, Basic Energy Sciences, Materials Sciences Division), NSF, and the Korean Institute for Advanced Study. Supercomputer time was provided by the National Center for Supercomputing Applications and the National Partnership for Advanced Computational Infrasture. M.S.C.M acknowledges support from CNPq-Brazil.

23 December 1999; accepted 9 March 2000

Tectonic Implications of U-Pb Zircon Ages of the Himalayan Orogenic Belt in Nepal

P. G. DeCelles,* G. E. Gehrels, J. Quade, B. LaReau, M. Spurlin

Metasedimentary rocks of the Greater Himalaya are traditionally viewed as Indian shield basement that has been thrust southward onto Lesser Himalayan sedimentary rocks during the Cenozoic collision of India and Eurasia. Ages determined from radioactive decay of uranium to lead in zircon grains from Nepal suggest that Greater Himalayan protoliths were shed from the northern end of the East African orogen during the late Proterozoic pan-African orogenic event. These rocks were accreted onto northern Gondwana and intruded by crustal melts during Cambrian-Ordovician time. Our data suggest that the Main Central thrust may have a large amount of pre-Tertiary displacement, that structural restorations placing Greater Himalayan rocks below Lesser Himalayan rocks at the onset of Cenozoic orogenesis are flawed, and that some metamorphism of Greater Himalayan rocks may have occurred during early Paleozoic time.

The Himalayan orogen includes four tectonostratigraphic units (Fig. 1) that record the tectonic evolution of northern Gondwana and southern central Asia since early Proterozoic time (*1, 2*). The Tibetan Himalaya comprises Cambrian through Eocene sedimentary rocks of the Tethyan succession (*3–5*). South of the Tibetan Himalaya lies the Greater Himalaya, consisting of high-grade metasedimentary rocks (*6–9*) intruded locally by early Paleozoic (*10–12*) and Miocene (*13–17*) granitoids. Greater Himalayan rocks are thrust southward along the Main Central thrust (MCT) on top of the Lesser Himalaya, which includes the ~10- to 12-km-thick Nawakot Group (Proterozoic) and Permian–lower Miocene strata (*18–24*). The Subhimalaya (Fig. 1) consists of Neogene foreland basin deposits. The Greater and Lesser Himalaya are sparsely dated, and their relationships to each other and to the Indian shield remain obscure. Because of their high metamorphic grade, Greater Himalayan rocks are assumed to be Indian shield basement that has been uplifted along the MCT. However, U-Pb ages and Nd isotopic data from Greater and probable Lesser Himalayan rocks in a small area near the MCT in central Nepal suggest that Greater Himalayan rocks may be younger than Lesser Himalayan rocks (*25*).

We conducted U-Pb isotopic analyses on 445 zircon grains (*26*) from 41 samples of the four Himalayan terranes and modern river sediment throughout Nepal (Fig. 1) to determine the ages, provenance, and crustal affinity of Himalayan rocks. Detrital zircons provide maximum depositional age constraints, and minimum depositional ages of some strata are constrained by U-Pb ages of cross-cutting intrusive rocks.

Ages of detrital zircons from quartzites in the Nawakot Group of the Lesser Himalaya are generally greater than ~1600 million years ago (Ma), with age distribution peaks at ~1866 and ~1943 Ma (Fig. 2). Because the age of zircons from the intrusive Ulleri augen gneisses is ~1831 Ma, the lower Nawakot Group must have been deposited between ~1866 and 1831 Ma. The detrital zircon ages are consistent with sedimentological data indicating that Lesser Himalayan sediments were derived from the Indian shield (*19, 21, 27*).

Metasedimentary rocks of the Greater Himalaya yield zircon ages of 800 to 1700 Ma,

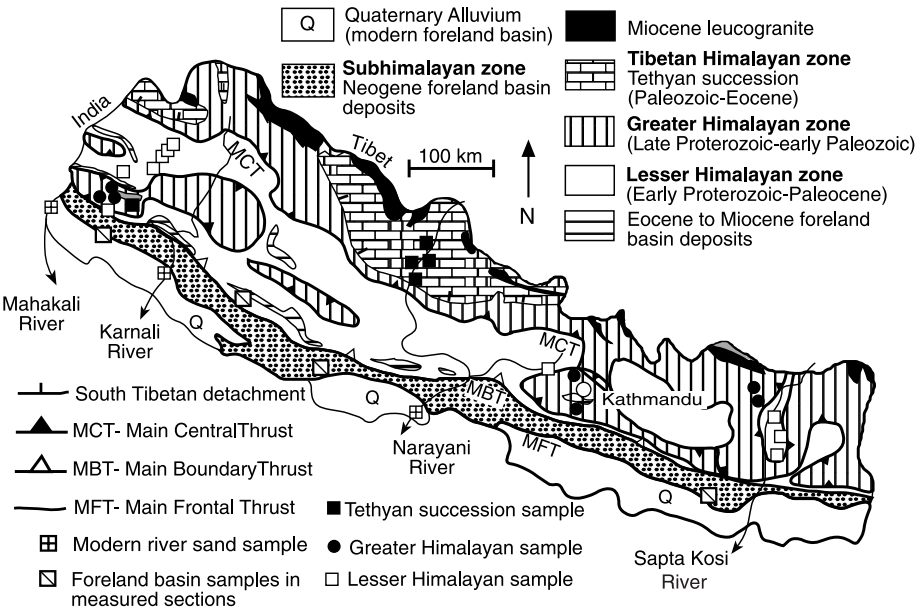

Fig. 1. Geologic map of Nepal, showing locations of samples and regional tectonostratigraphic terranes.

Department of Geosciences, University of Arizona, Tucson, AZ 85721, USA.

*To whom correspondence should be addressed. E-mail: decelles@geo.arizona.edu